CEWES MSRC/PET TR/98-15

Coupling of Circulation, Wave and Sediment Models

by

S. Zhang
David Welsh
K. Bedford
P. Sadayappan
S. O'Neil

DoD HPC Modernization Program
Programming Environment and Training
CEWES MSRC

04h00398

Work funded by the DoD High Performance Computing Modernization Program CEWES Major Shared Resource Center through

Programming Environment and Training (PET)

Supported by Contract Number: DAHC 94-96-C0002
Nichols Research Corporation

Climate, Weather and Oceanography
Focused Effort Year 2 Progress Report
Coupling of Circulation, Wave and Sediment Models

S. Zhang*, D. Welsh*, K. Bedford*, P. Sadayappan† and S. O'Neil*

March 31, 1998

Abstract

This report summarizes the progress and accomplishments made on Focused Effort No. 1 by the CWO-CEWES group at The Ohio State University (OSU) for the CEWES MSRC-CWO project under the DoD HPCMP during Year 2 (April 1, 1997 - March 31, 1998). This focused effort concentrates on the physics and coupling of circulation, wave and sediment codes for coastal region dynamics. The implementation and computational testing of the coupled codes are made using Lake Michigan as the modeling domain. Three codes; CH3D, WAM and CH3D-SED have been modified and deployed for the lake. Both one-way and two-way couplings have been made between WAM and CH3D. The dynamical effects of wave-current interactions at the surface are reported for demonstration examples. Wave-current coupling in the benthic boundary layer will be included in the follow on Year 3 of this project. Table 1 summaries the tasks which have been completed. A website has been constructed at OSU (URL *http://superior.eng.ohio-state.edu/∼sxz/CEWES.html*) to show results as the coupling progresses, and is updated frequently as new results are obtained.
The authors would very much like to thank Drs. Billy Johnson and Bob Jensen for their support and help in getting our group up to competence in the WAM and CH3D-SED codes; and Drs. David Huddleston, Jianping Zhu, and Purushotham Bangalore at Mississippi State University for providing the CH3D parallel version. The authors would especially like to thank Dr. Carey Cox, our on-site CWO scientist, who has now left to pursue a career in academia. His help was pivotal and will be missed.

1 Introduction

Objective of this CEWES MSRC-CWO focused effort is to develop the physics and parallel computing tools necessary to fully couple wind-wave, circulation and sediment transport models. Such integrated tools will be required in support of high resolution prediction of nearshore and harbor activity in support of troop deployment operations, and prediction in support of public works activities at WES.

*The Ohio State University, Department of Civil and Environmental Engineering and Geodetic Science
†The Ohio State University, Department of Computer and Information Science

1.1 Experiment Site

Lake Michigan was chosen as the experimental site for the computational coupling of CH3D and WAM for two important reasons; that the lake is a closed domain, and that it is currently the site of an extensive field measurement and modeling program. By the use of a closed computational domain, boundary conditions are simple to implement correctly. The field measurement program provides both temporally and spatially dense physical, chemical and biological data which will be used for model comparison and verification.

If the model domain had a large open boundary, then special provisions must be made when using computational models based on the shallow-water equations (the hydrostatic, Navier-Stokes equations applied on a rotating planet). At an open boundary the surface height, current and constituent values must all be specified, from the surface to the bottom if the flow is incoming towards the domain, or the boundary values must be radiated out for outgoing transport. These boundary conditions introduce error, since there is no way of knowing what the incoming values should be. Furthermore, simply specifying values at the open boundary can lead to the introduction of spurious surface elevation waves to be reflected off the boundary and back into the modeled flow domain. Closed boundaries are much simpler to implement, since no flow can occur at or through such a boundary. By selection of a closed domain the coupling issues are addressed and examined without the confusion of ambiguous results from poor boundary conditions.

As to the field program, the National Science Foundation (NSF) through the Coastal Ocean Processes (CoOP) program and National Oceanic and Atmospheric Administration (NOAA) through the Coastal Ocean Program (COP) are co-sponsors of the Episodic Events - Great Lakes Experiment (EEGLE); see the URL *http://www.glerl.noaa.gov/eegle* for more details of the project. The purpose of the project is to collect extensive data sets of surface wave height and frequency, as well as profiles of current, temperature and suspended sediment concentration. Since the research program will span three seasons of intensive data collection when completed, the extent of the data products will allow for thorough model comparison and tuning to be conducted.

1.2 Physics of Coupled Waves and Currents

The principle reasons for coupling a current or circulation model with a surface wave model are found in the physical interactions taking place in the surface boundary and bottom boundary layers. At the surface, a wave model will provide a modification of the wind-induced surface stress, and the radiation stress terms will allow for adjustments to the water level, or barotropic mode. The wave model will also make adjustments due to current-induced wave refractions as well as depth adjustments from depth-induced refraction. Finally, the currents from the circulation model provide additional source/sink terms which modulate the wave model frequency space.

The bottom boundary layer is also influenced by wave induced stresses computed by WAM which are passed back to CH3D, the circulation model. In the bottom boundary layer, the current-induced and wave-induced bottom stresses may be directed in different, even opposing directions. The resuspension, entrainment and deposion processes of bottom sediments is nonlinearly related to the relative magnitudes of the wave- and current-induced bottom stresses (Glenn and Grant, 1987). Thus, determining and properly resolving the relative magnitudes of the two stresses is important to properly applying the wave-current bottom boundary condition.

1.3 Task Summary Calendar

Table 1 gives a brief summary on the tasks that we have carried out during Year 2 (04/01/97 - 03/31/98) for the CEWES MSRC-CWO project under the DoD HPCM.

Table 1: Tasks finished in 1997

Task	**Completion Date**
Deploy WAM-s[1] in Lake Michigan	10/97
Deploy CH3D-s in Lake Michigan	10/97
Parallel WAM (WAM-p)	2/98
Deploy CH3D-p in Lake Michigan	12/97
Modify CH3D-s to include heat transport	11/98
Deploy, modify CH3D-SED-s for Lake Michigan	3/98
Modify WAM-s to include unsteady current	1/98
Modify CH3D-s to include wave's effects	1/98
One-way coupling of WAM-s with CH3D-s	1/98
Two-way coupling of WAM-s with CH3D-s	3/98

[1] WAM-s refers to the sequential version of WAM, CH3D-p refers to the parallel version of CH3D, etc.

2 CH3D, CH3D-SED and WAM Applied to Lake Michigan

Towards the objective of developing an integrated coastal simulation system, we first employed and modified the individual codes available from CEWES in order to independently model current circulation, heat, sediment transport processes and surface waves in Lake Michigan. The results obtained from these independent runs are used as ground truth. Introducing new processes and modifying the physics of the models, as well as effecting a model coupling, should more realistically model the dynamic processes which occur in the lake.

2.1 CH3D

The sequential CH3D code (CH3D-s) has been developed to predict three-dimensional solutions of flow velocity components, temperature, salinity and free-surface water elevation through solving the conservation equations of mass, momentum and energy in curvilinear (horizontal direction), sigma stretched (vertical direction) coordinates, using the Boussinesq and hydrostatic approximations (Chapman et al., 1996; Johnson et al., 1991). The physical processes impacting the circulation computation include tides, wind, density variations due to temperature and/or salinity, fresh water inflow, turbulence, and the effect of the earth's rotation. A two-equation vertical (k-ϵ) turbulence closure scheme (ASCE Task Committee on Turbulence Models in Hydraulic Computation, 1988) is incorporated to determine the vertical eddy viscosity.

The curvilinear coordinate feature of the CH3D model in the horizontal dimensions provides the grid resolution enhancement, which is necessary to adequately resolve deep navigation chan-

nels and irregular shoreline configuration. The solution algorithm employs the external and internal mode splitting approach. The external mode consists of vertically averaged equations, which provide a solution for the free surface displacement and vertically averaged velocities. The internal mode computes the deviation of the horizontal components of the full 3D velocity from the vertically averaged ones. In addition, the vertical component of the 3D velocity, 3D temperature and salinity are also computed in the internal mode. More detailed description about the CH3D code can be found in Chapman et al. (1996).

2.1.1 Deployment of Sequential CH3D-s in Lake Michigan

In late September of 1997, we received the CH3D-s and its test input data for New York Bight. Before the CH3D-s was deployed to Lake Michigan, we performed several tests for New York Bight by changing several important dynamic parameters (different input wind fields, UREF, HMIN, EXP, AVH, etc.) either in the code or in the input file. The objective was to determine under what conditions the CH3D code ran well for the given case and which part of the code was not included in the computation. It was found that no temperature and salinity computations were involved in the CH3D code given to us. The following gives a detailed description of the deployment of CH3D-s for Lake Michigan:

Examination of the CH3D-s code. In order to master the construction of the code and correctly understand the physical meanings of each subroutine, we have re-derived all the analytical expressions for the external modes and internal modes of the governing equations, from which the numerical solutions are obtained. Then, we went through each of the subroutines to determine each of the analytical expressions was implemented in the code and understand the details about how they were coupled to each other according to the user's guide by Chapman et al. (1996).

Generalization of the hardwired code. Since the version of the CH3D-s we received was deployed for New York Bight, there were many hardwired codings which were configured only for that particular site and which must be changed or deleted when the code is deployed to a different water body (here Lake Michigan). The reconfigured hardwired codings for Lake Michigan include (i) selected input parameters, (ii) the x-, y- coordinates of tidal boundaries, (iii) the river inflow and its related input, (iv) the wind-observation locations and the wind stress computing subroutine, (v) the zeros, which were explicitly specified for `HS(I,J)`, `HU(I,J)` and `HV(I,J)` at certain cells; (vi) several if-then statements were inserted in the code due to the special geometry character of New York Bight. We also modified the output format and location for the purpose of post-processing the output using the existing visualization and graphic tools at OSU.

Inclusion of heat transfer in the circulation computation. From the hydrodynamical standpoint, it is essential to include the thermal effects in the circulation process, especially for Great Lakes (Bedford and Schwab, 1998, 1994). However, the temperature computation in CH3D-s given to us was offline and there were no data available for us to verify the temperature computation for the test case of New York Bight. In order to meet the needs of including the thermal effects, we first modified the CH3D-s code so that the temperature variations can be predicted in the hydrodynamic simulation of Lake Michigan. The modifications includes (i) configuration of the correct

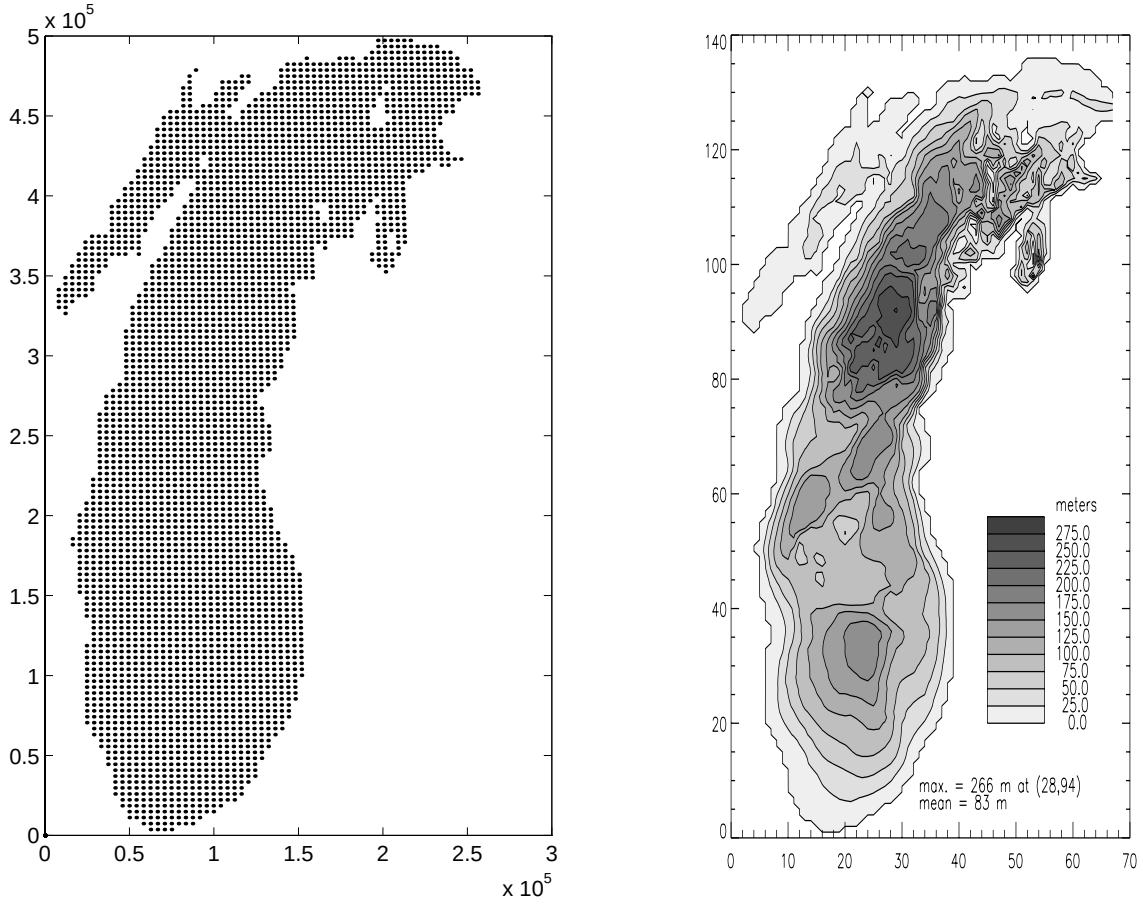

Figure 1: Lake Michigan grid (left), with axis units in meters, and contoured smoothed bathymetry (right), with axis units in grid cells.

common blocks for the temperature solver, (ii) adjustment of the temperature and heat flux distribution at the water surface and (iii) adjustment of the eddy diffusivity. Then, we ran a comparison test between the CH3D-s and POM codes (Blumberg and Mellor, 1987) in simulating the internal Kelvin waves and coastal upwelling fronts as observed in Lake Michigan (Mortimer, 1963). The simulation results will be reported in the demonstration example of Section 2.1.3.

Generation of grid-mesh. Like any numerical modeling, the grid-mesh generation is one of the fundamental part of the hydrodynamic simulation of the Lake Michigan. According to the CH3D User's Guide (Chapman et al., 1996), another code named 'WESCORA' should be used to generate the grid meshes. However, we did not have access to that code. We followed the grid-mesh example of N.Y. Bight to generate 2×2 km and 4×4 km horizontal grid meshes covering Lake Michigan. Figures 1 (left) were generated on the basis of the bathymetry data-set with 1 meter vertical contour resolution. The bathymetry map is shown in Figure 1 (right). The bathymetry data is discussed in Section 2.3.1.

The following lists the key elements in the grid-mesh generation, which were not described in the CH3D-s user's guide:

(*i*) CH3D requires an $N \times M$ horizontal grid mesh covering the entire water body, with N and M being the grid number in x- and y-directions, respectively. The grids can be unequally displaced in each direction.

(*ii*) The water depth at the grid cell corners must be specified. Zeros are specified for land grids.

(*iii*) For the grids located in the water portion, the x-y coordinates are specified according to their relative position (scaled in feet).

(*iv*) For the grids on the land side, a big number (9×10^{10}) is assigned to replace their x and y coordinate values.

(*v*) The vertical depth at each grid in the water region is transformed using the sigma-stretched scheme. K sigma-layers with unequal thickness are specified in the vertical direction (K equal to 13, 17, and 20 has been tested).

2.1.2 Deployment of Parallel CH3D-p in Lake Michigan

In begin of December, 1997 we received the first parallel version of the CH3D code , which were tested on the SGI O2K and for the test case of New York Bight. The computation was parallelized by decomposing the y-dimension of the spatial domain. The common-blocks structure was identical to that as used in the sequential CH3D code while the MPI was used to make the computation in parallel. The I/O was made on the zeroth process and read-in data were BROADCAST to every process. We first installed the CH3D-p on the SGI Power Challenge running at the Ohio State Supercomputer Center (OSC), which is a multi-user machine and has a memory of 2 GB. After several tests, it was found that it is difficult to run the CH3D-p on this machine even for the test case with a grid mesh of 51×76×10 because a memory of 55 MW is essential to run this job on one process. Then we asked for the CRAY T3E version of the CH3D-p.

Test the CH3D-p on CRAY T3E for New York Bight. In the early January of 1998, we received a CRAY T3E version of the CH3D-p and then installed it on the CRAY T3E running at the OSC. However, we were not able to make the code run smoothly. It kept generating the errors of floating exception randomly here and there in the code. Some time were spent debugging the code. Later, working together with Purushotham Bangalore we found the initial MPI set up was not compatible with the choose of the process number. After this problem was fixed, the CH3D-p started run on the OSU CRAY T3E for the given test data. As usual, several tests were performed to check whether every subroutine and section of the code can be involved in the computation. It was found that no temperature and no salinity computations were included in the CH3D-p code.

Deployment of CH3D-p in Lake Michigan. Same procedure as described in Section 2.1.1. was followed to apply the CH3D-p to lake Michigan. In addition, we also changed the initial MPI set up. However, the CH3D-p blows up after running several time steps. We suspects the blow-up was caused by the memory limitation of a single process of CRAY T3E, which is 16 MW. The grid-size of Lake Michigan is 67×139×20, which is more than twice of the New York Bight grids.

The current CRAY T3E version of the CH3D code uses an identical common-blocks structure to that as used in the CH3D-s code. In this parallelization strategy of non-localization memory

for each process, the same memory as that used for running a sequential job is declared for every processor, but that memory is much greater than what the process actually needs. Obviously, non-localization memory for each process causes in-efficient use of memory space. An explicit partitioning of the data into separate address space of each process is essential to solve memory efficiency problem and to run a big application job.

2.1.3 Test Case Results

Simulation of an internal Kelvin wave/coastal upwelling front in Lake Michigan. Comparison tests were performed using the published results by Beletsky et al. (1997) of simulating the internal Kelvin waves and coastal upwelling fronts. They were well known hydrodynamic phenomena in Lake Michigan (Mortimer, 1963) and represent an extreme test of the model's performance in calculating the stratified flow. The objectives are two fold: one is to examine the capability of the modified CH3D-s code in reproducing robust thermo-dynamical phenomena; The second is to tune the physical parameters and dynamic options specified either inside the code or through the input files, to conditions more representative of those in Lake Michigan. In the following, we will briefly describe the model set-up and results. Interested readers can read the paper by Beletsky et al. (1997) for a detailed description of the physics and technical issues.

Two grid sizes (4 and 2 km) were used for this study. The 2 km grid mesh is built up in the Cartesian coordinate with $\Delta x = \Delta y$. The 4 km grid is in spherical coordinates with $\Delta\theta = 0.03333^\circ$ and $\Delta\phi = 0.05^\circ$, where θ and ϕ are the longitude and latitude. The 2-km grid mesh consists of 127 $\times$ 250 grid points and the 4 km one has 67 $\times$ 139 points shown in Figures 1 (left). In the figure the grid sizes in the latitude nd longitude directions are 3.7 km and 3.9 km, respectively. The coordinates of the lower-left corner are (-88.1,41.6) and the top-right corner are (-84.7,46.2). The bathymetries shown in Figures 1 (right) were modified using a topographic smoothing subroutine from the POM code so that the depth ratio of any two adjacent grids does not exceed 0.5 in order to satisfy the hydrostatic consistency criteria for the σ coordinate (Haney, 1991). In the vertical coordinate, 20 σ layers are used with denser grids distributed towards the surface in order to get a good resolution for the presence of thermocline. We also ran a simplified test, in which we assume the lake is 100 m depth with a flat bottom.

The simulation is driven by a simplified wind field, which exists in the first day and becomes to zero during the rest of the simulation period. Spatially, the wind is from the north and uniformly distributed. Figure 2 (left) shows an example, in which the wind increases linearly from zero to its maximal amplitude (5 m/s) over 6 hour, remains at this maximum value for another 18 hours and then decreases to zero in the next 6 hours.

Figure 2 (right) shows the initial temperature condition, which represents the thermocline commonly observed in the Great Lakes during summer and early fall. An isothermal layer of 21.4 $^\circ$C is specified for the top 11 m. The temperature decreases to 7 $^\circ$C linearly from 11 m to 20 m. From 20 to 90 m, the temperature decreases to 4.5 $^\circ$C and remains this value for greater depth. Zero heat flux is specified at the water surface, bottom and also the lateral boundaries.

The simulation starts from no motion and zero surface displacement for the given wind forcing and initial condition shown in Figure 2. The total simulation time is 15 days with time increment of 2 minutes at each time step. Because the purpose of performing this test is verifying the modified CH3D-s code, especially the temperature solver, we did not use the same wind fields as in Beletsky

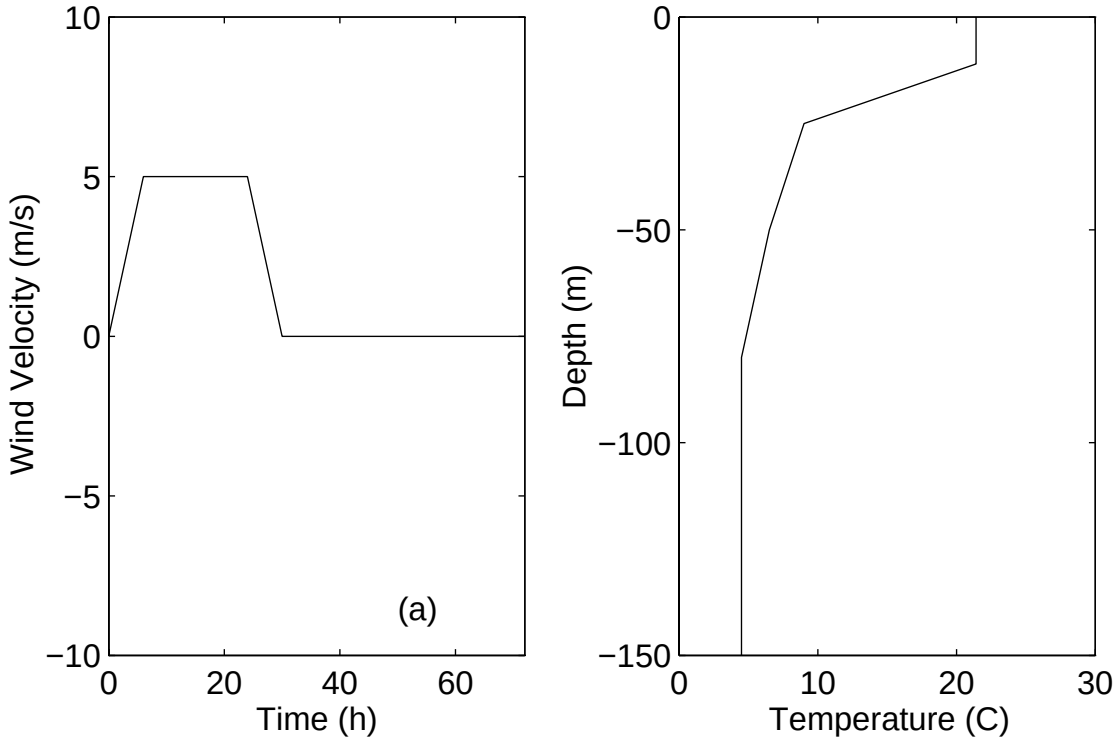

Figure 2: Temporal variation (left) of the northern wind and initial temperature profile (right) used in the Kelvin-wave simulation.

et al. (1997). Nevertheless, the internal Kelvin waves and coastal upwelling fronts are produced in the simulation using the CH3D-s.

Figures 3 shows the temporal variations of temperature field at the depth of 13 m at the starting time, 1.2 day, 5 day and 10 day of the simulation time. One can observe the appearance of the eastern upwelling (indicated by the darkest shading) and its northward migration along the eastern shore.

Two quicktime format movies from this simulation may be found at the previously mentioned website (URL *http://superior.eng.ohio-state.edu/∼sxz/CEWES/focused.html*), showing the water elevation and temperature variations at 13 m depth associated with the Kelvin-wave propagation.

2.2 CH3D-SED

The sequential CH3D-SED code, CH3D-SED-s, is an extension of CH3D-s, into which a sediment module has been coupled. Given the local flow conditions, the sediment module computes the mobile-bed processes including aggradation and scour, bed-material sorting, and movement of both bedload and suspended load of non-uniform sediment mixtures. Sediment computations consist of both suspended and bed load prediction and are based on the solutions of: (i) a two dimensional mass-conservation equation for a particular size class of active-layer bottom sediment; (ii) a two dimensional global mass-conservation equation for bed sediment with different size classes; and (iii) a three dimensional advection-diffusion equation for suspended sediment transport of each size class, together with several well-tested auxiliary relationships, which pa-

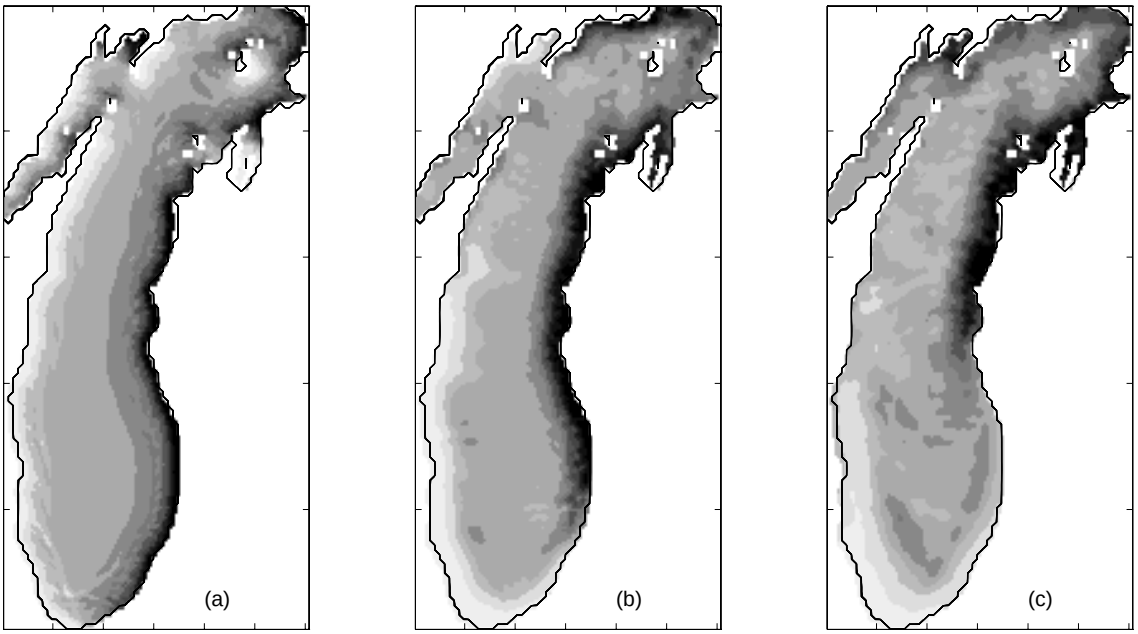

Figure 3: Temporal variations of temperature (°C) at depth of 13 m associated with the Kelvin-wave propagation at 1.2 days, 7 days, and 10 days (from left to right). The darkest areas indicate a temperature below 12 °C, and the lightest shade indicates a temperature greater than 20 °C.

rameterize the source-sink terms in the governing equations. Similar to the CH3D-s code, the equations are solved in the curvilinear coordinates (Spasojevic and M. Holly, 1994).

The sediment-operations developed for the CH3D-SED-s fully communicate and with the rest of the CH3D-s code at every time step and therefore the sediment and wind-driven circulation fields are fully coupled. The hydrodynamic operations of CH3D-s provide all the necessary hydrodynamic input required by the computation of sediment transport (e.g., local velocities and water depth). The sediment module, in turn, communicates changes in bed elevation (i.e., the depth), bed-surface size-distribution (i.e., the friction coefficients), and density (due to the presence of suspended sediment) back to CH3D-s hydrodynamics operations. Computationally the sediment module and the rest of the CH3D-SED-s code are also compatible with each other. For example, the same QUICKEST numerical scheme has been used in solving both the sediment concentration equation and temperature and salinity equations. Detailed documentation of the coding and use of mobile-bed capability in the CH3D-SED-s can be found in Spasojevic and M. Holly (1994).

2.2.1 Deployment of CH3D-SED-s in Lake Michigan

In the late November of 1997, we received the sequential version of CH3D-SED-s code and the related input data for the Mississippi River test case. After a few simple tests on the SGI Power Challenge making sure that the code ran well for the given input data, we started the deployment of this code to Lake Michigan. We first tested its hydrodynamics operation and then activated the sediment module.

Comparison CH3D-SED-s and CH3D-s hydrodynamic computations. We first changed the

hardwired code in CH3D-SED-s, which were set for the Mississippi River. This was done in the same way as described in Section 2.1.1 for the CH3D-s code. We also modified the CH3D-SED-s code so that the heat transport process is included in the sediment-circulation coupled system. This modification was made because no temperature computation had been involved in the studies of Mississippi River (Dr. Dan Gessler, personal communication, December of 1997). In addition, we systematically (or line by line) compared the CH3D-SED-s with CH3D-s. The objective was to identify the differences (if any) in the hydrodynamic computation.

It was found that the hydrodynamics operation of the CH3D-SED-s are the very same as those of CH3D-s except that in the original CH3D-SED-s code (i) the wind fields were assumed to be spatially uniform, (ii) the vertical eddy diffusivity was not updated at each time step, and (iii) the bottom boundary condition specified for solving the three-dimensional velocity components is slightly different. Then we added two subroutines to the CH3D-SED-s code; one subroutine accommodated the temporal and spatial variability of wind fields, while the other updated vertical eddy diffusivity and its variations at each time step using the formula relating the vertical eddy diffusivity to the vertical eddy viscosity (Equation 46 in Chapman et al., 1996).

After making these modifications, we independently ran the two codes for Lake Michigan using the same wind input. Under the condition of no sediment transport, the CH3D-SEDss code generates the same results in the water velocity components and temperature as those generated by the CH3D-s, indicating that the hard wired codings in both of the codes were correctly changed.

Inclusion of sediment computation. The next test we made was to activate the sediment module for Lake Michigan. In the first several tests, the sediment module malfunctioned, three problems were identified.

One problem was associated with the 1-D channels, which horizontally consist of only two non-land grids. Over these grids the subroutine `DIMVEL` generated errors of floating exceptions due to the zero water depths of the neighboring grids on the land side. To fix this problem, the subroutine `DIMVEL` has been modified such that over the 1-D channel the land-side grids would not be included in the computation.

The second problem was due to the hardwired set-up associated with the River and Tidal boundaries specified for Mississippi River in subroutine `SBINFO`. This problem was easily fixed by commenting out the hardwired set-up lines.

The third problem was due to a high-gradient bathymetry condition. This resulted in the parameterized thickness of the active-layer greater than that of the lowest sigma-layer in some locations near the small islands. For solving this problem, one can artificially increase the water depth by a couple of meters at these locations or increase a little the thickness of the bottom layer through adjusting the sigma value. If the latter was chosen, one must recompile the code. Also, please note the trade-off issue between the parameterized thickness of the active-layer and the thickness of the bottom sigma layer. In the near future, we will calibrate and modify the transport equations used in the current CH3D-SED-s version so that they can better describe the sediment transport in Lake Michigan regions with active bedload transport. After fixing these problems in the sediment module, the CH3D-SED-s runs stably for Lake Michigan on the SGI Power Challenge.

2.2.2 Deployment of CH3D-SED-p in Lake Michigan

This version of the model has not been available as of 02/16/98. This portion of the project will be initiated and completed in Year 3.

2.2.3 Test Case Results

As with the previous section, this portion of the project will be initiated and completed in Year 3.

2.3 WAM

The WAM model simulates the growth, evolution, and decay of wind-waves across a numerical grid. The first version, or "cycle", of the model is documented in WAMDI (1988). The most recent "frozen" version is cycle 4 (Gunther et al., 1992). Cycle 4 is the first version to be based on the conservation of wave action density, rather than wave energy density. This modification simplified the inclusion of current effects on waves. The development, algorithms, and verification of the model are discussed at length in Komen et al. (1994).

WAM is classified as a third-generation wave model due to the sophisticated and realistic treatment of the nonlinear wave-wave interaction source term. The model includes all significant shallow water effects and has a spectral structure in which the evolution of each component in a two-dimensional, frequency-direction array is modeled independently. WAM requires inputs of wind fields, bathymetry, and (optionally) a current field. Outputs can be tailored to include maps of the various common parameters (e.g. significant wave height, mean wave direction, peak frequency, swell height), and parameter time series and two-dimensional energy spectra at selected locations. The sequential (i.e. single processor) version of WAM has been available for use at CEWES MSRC for a number of years. A parallel version of the code was first developed by John West under a CHSSI project. Optimization and enhancement of features of the parallel WAM (WAM-p) code are being undertaken as part of the core task of the PET CWO effort (Welsh et al., 1998).

2.3.1 Deployment of Sequential WAM-s in Lake Michigan

The Lake Michigan WAM-s deployment uses a 3 minutes longitude by 2 minutes latitude, spherical co-ordinate computational grid. This corresponds to approximately 4 km square cells; the dimensions of the grid are 67 cells in the East-West direction by 139 cells in the North-South direction. This size of grid was selected to keep CH3D memory requirements within the bounds of rapid turnaround queues on the CEWES CRAY C916 computer. The bathymetry was resampled from the National Oceanic and Atmospheric Administration (NOAA) 9 arc second Lake Michigan bathymetry database (see URL *http://www.ngdc.noaa.gov/mgg/fliers/96mgg03.html*). The maximum depth in the grid is 262 m.

The standard number of WAM-s spectral components were used: 25 bins in frequency-space and 24 bins in direction-space, giving a total of 600 components. The lowest frequency was set to 0.06 Hz, which is appropriate for the fetches, depths, and wind speeds encountered in Lake Michigan. The ratio between successive component frequencies was kept at the standard value of 1.1, giving a maximum frequency of 0.59 Hz. A suitable time step for the grid and frequency coverage was found to be 1 minute.

The WAM-s model uses a blocking approach in which the bathymetry grid can be divided into a number of East-West aligned blocks, or slices. This allows a dramatic reduction of the memory requirement, and also foresees parallelization of the code. For reasons of computational efficiency the maximum number of cells per block should be set to a power of two. There are 3932 water cells in the Lake Michigan grid, and 2 blocks, with a maximum number of 2048 cells per block, were selected. This resulted in a memory requirement close to 6 Mw, which kept WAM-s simulations within the 8 Mw batch job queue. An 8 block deployment was also tested, to ensure that the use of multiple blocks did not reveal programming errors or alter results. The Lake Michigan WAM-s deployment requires approximately 1200 CPU seconds for every 24 hours of simulation on the CEWES CRAY C916.

WAM-s can be deployed using a spherical or Cartesian grid. A spherical grid was selected in this case since comments in the code listing indicate that the model has been more extensively tested for that option.

2.3.2 Deployment of Parallel WAM-p in Lake Michigan

This version of the model has not been available as of 02/16/98. This portion of the project will be initiated and completed in Year 3.

2.3.3 Test Case Results

An idealized test case was designed to show the effects of the various CH3D-s/WAM-s coupling mechanisms implemented in this project. An idealized test is more useful than a hindcast at early stages of the coupling development since simple wind fields permit the influence of particular algorithms to be more clearly identified. The test case used involved wave growth, rotation, and decay, with a wind field read in hourly. The wind was ramped up from zero to 10 m/s, N over 6 hours, then held constant for 30 hours. Wind direction was then backed to W over 6 hours, followed by a second 30 hour steady wind period. Wind speed was then ramped down to zero over 6 hours, with a final 6 hour period of no wind. Total test duration was 84 hours and initial conditions were quiescent. The test was named “I1S1”, with “S1” (stage 1) indicating stand-alone (uncoupled) models.

In this section some test results are shown for WAM-s test I1S1. The results confirm the realistic behavior of the basic Lake Michigan deployment and serve as a baseline for comparisons with the later coupling stage versions: “S2” will be used to indicate one-way coupling between CH3D-s and WAM-s, with each model reading arrays from a file generated by the S1 run of the other model. “S3” will be used to indicate two-way coupling, where the models run simultaneously and pass arrays in a synchronized manner.

Figure 4 shows a plot of significant wave height, H_s, at hour-36; wave vectors are also shown, with their lengths normalized using the maximum lakewide wave height. Typical fetch-limited growth is evident and refraction and lateral energy spreading can also be seen close to shore.

Figure 5 shows a time series of H_s at detailed output station number 8, located at grid point (23,16). The depth at this station is 60 m. The steady-state wave height is seen to be lower for the W wind than for the N wind. This is due to a reduced fetch and increased bottom friction due to lower upwind depths.

Figure 6 shows a time series of mean wave direction, $\overline{\theta}$, at station 8. A realistic, smooth sea

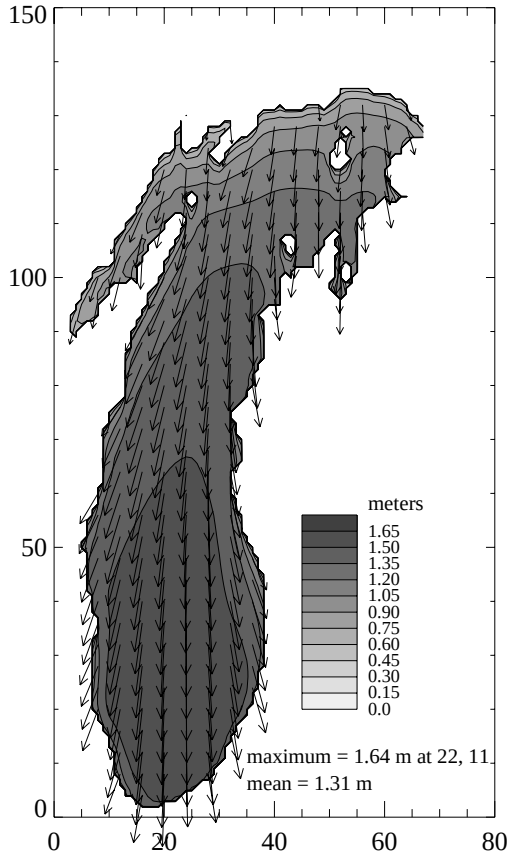

Figure 4: Significant wave height contours at hour-36 of test I1S1

rotation is evident. It is also noticeable that the steady-state $\overline{\theta}$ do not match the prevailing wind directions precisely. This is caused by the refraction and spreading effects mentioned above. These effects become more dominant after hour-72, when the wind input is reduced.

3 The Coupling of the CH3D and WAM Models

3.1 Effects of currents on waves

3.1.1 Propagation effects

The governing equation of the WAM-s cycle 4 model is the spectral action density conservation equation in spherical co-ordinates:

$$\frac{\partial N}{\partial t} + \frac{\partial(\dot{\lambda}N)}{\partial \lambda} + \frac{\partial(\dot{\phi}N)}{\partial \phi} + \frac{\partial(\dot{\sigma}N)}{\partial \sigma} + \frac{\partial(\dot{\theta}N)}{\partial \theta} = S'_{in} + S'_{nl} + S'_{ds} \quad (1)$$

where $N = N(\sigma, \theta, \lambda, \phi, t)$; θ is measured clockwise from North; λ is longitude; ϕ is latitude; the dotted terms are partial derivatives with respect to time; $S'_{in} = S'_{in}(\sigma, \theta, \lambda, \phi, t)$ is the wind input

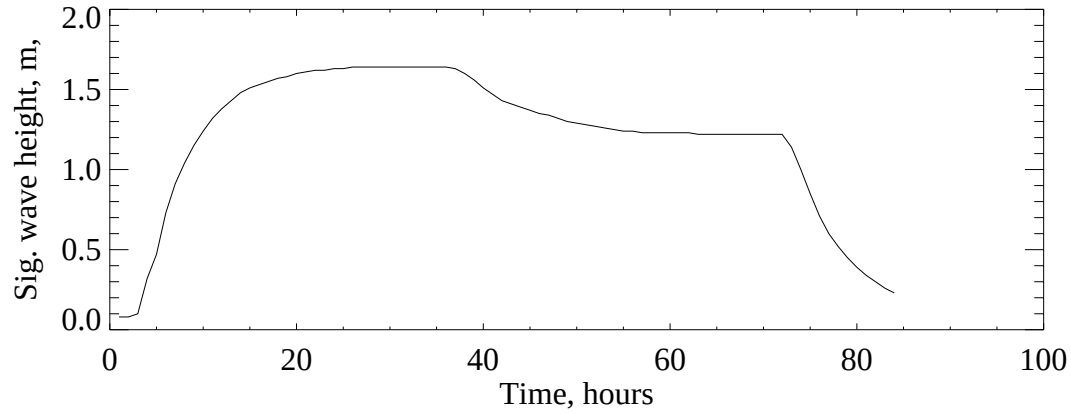

Figure 5: Significant wave height time series at station 8 for test I1S1

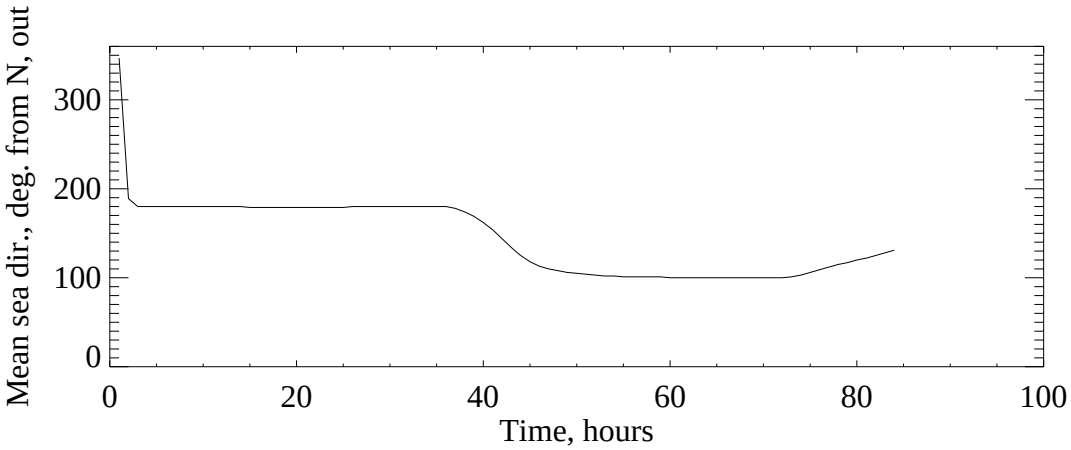

Figure 6: Mean wave direction time series at station 8 for test I1S1

source term; S'_{nl} is the nonlinear interaction source term; and S'_{ds} is the dissipation sink term. This equation is in terms of the relative frequency, σ, (for a frame of reference moving with the local current), given by

$$\sigma \;=\; \sqrt{g\;k\;\tanh(kh)} \tag{2}$$

where k is the scalar wavenumber and h is the depth. σ is related to the absolute frequency, ω, (for a fixed frame of reference), by

$$\omega \;=\; \omega - \boldsymbol{k}\cdot\boldsymbol{U} \tag{3}$$

where $\boldsymbol{U}$ is the current vector. The time derivatives in (1) are given by

$$\dot{\lambda} \;=\; (c_g \sin\theta \;+\; U_\lambda)\;(R\cos\theta)^{-1} \tag{4}$$

$$\dot{\phi} \;=\; (c_g \cos\theta \;+\; U_\phi)\; R^{-1} \tag{5}$$

$$\dot{\sigma} \;=\; \frac{\partial \sigma}{\partial h}\big(\boldsymbol{U} \cdot \Delta h\big) \;-\; c_g\big(\boldsymbol{k} \cdot \frac{\partial \boldsymbol{U}}{\partial s} \tag{6}$$

$$\dot{\theta} \;=\; \dot{\theta}_g \;+\; \dot{\theta}_d \;+\; \dot{\theta}_c \tag{7}$$

$$\dot{\theta}_g \;=\; (c_g \sin\theta \tan\phi) R^{-1} \tag{8}$$

$$\dot{\theta}_d \;=\; \left[\sin\theta \frac{\partial h}{\partial \phi} \;-\; \frac{\cos\theta}{\cos\phi}\frac{\partial h}{\partial \lambda}\right] \frac{\partial \sigma}{\partial h}\,(kR)^{-1} \tag{9}$$

$$\dot{\theta}_c \;=\; \left[\sin\theta\big(\cos\theta \frac{\partial U_\phi}{\partial \phi} \;+\; \sin\theta \frac{\partial U_\lambda}{\partial \phi}\big) \;-\; \frac{\cos\theta}{\cos\phi}\big(\cos\theta \frac{\partial U_\phi}{\partial \lambda} \;+\; \sin\theta \frac{\partial U_\lambda}{\partial \lambda}\big)\right] R^{-1} \tag{10}$$

where R is the radius of the Earth, s is in the direction of the wave component, and $\dot{\theta}_g$, $\dot{\theta}_d$, and $\dot{\theta}_c$ are the grid, depth, and current refraction terms, respectively.

For reasons of familiarity and consistency with data, WAM cycle 4 outputs energy density spectra with respect to the fixed frame of reference, $E(\omega, \theta)$. These spectra are obtained using

$$E(\sigma, \theta) \;=\; N(\sigma, \theta) \cdot \sigma \tag{11}$$

then $E(\omega, \theta)$ is interpolated from $E(\sigma, \theta)$ based on (3).

The importance of currents in the WAM model is evident from the presence of $\boldsymbol{U}$ in (4), (5), (6), and (10). Equations (4) and (5) include wave propagation by currents; (6) describes modulation in σ-space; and (10) represents wave refraction by currents.

3.1.2 Source/sink term effects

The source/sink terms in WAM cycle 4 are calculated using algorithms derived for the evolution of $E(\omega, \theta)$ components and included in WAM cycle 3 (the form of each source/sink algorithm is detailed in Komen et al. (1994)). For example, $S'_{in}(\sigma, \theta)$ is calculated using

$$S'_{in}(\sigma, \theta) \;=\; \frac{S_{in}(\sigma, \theta)}{\sigma} \tag{12}$$

where the $S_{in}(\sigma, \theta)$ algorithm is identical to the $S_{in}(\omega, \theta)$ scheme used previously. It is unlikely, however, that the same set of source/sink algorithms hold in the presence of currents, but the lack of wave evolution data with respect to a moving frame of reference has hindered the development of alternative expressions. In the absence of suitable data one can attempt to modify the existing algorithms. Tolman (1991) did this using a Jacobian transformation of each term:

$$S'_{in}(\sigma, \theta) \;=\; \frac{1}{\sigma}\left(1 \;+\; \frac{\boldsymbol{e}_s \cdot \boldsymbol{U}}{c_g}\right)^{-1} S_{in}(\omega, \theta) \tag{13}$$

where $\boldsymbol{e}_s$ is a unit vector in direction θ. This may be a qualitatively correct approach for the wind input term, but consideration of each of the source/sink mechanisms suggests that a single adjustment strategy is not suitable for all of them.

For wind input the critical factor is the relative motion of the wind with respect to the wave roughness elements (individual waves). It is, therefore, reasonable to assume

$$S_{in}\big(\sigma = \omega_1, \theta, \boldsymbol{u}_{rel} = \boldsymbol{u}_1\big) \;=\; S_{in}\big(\omega = \omega_1, \theta, \boldsymbol{u}_{rel} = \boldsymbol{u}_1\big) \tag{14}$$

It follows that the standard WAM algorithm can be used here if the 10 m wind velocity is also adjusted to the moving frame of reference:

$$\boldsymbol{u}'_{10} \;=\; \boldsymbol{u}_{10} \;-\; \boldsymbol{U} \tag{15}$$

One then obtains

$$S'_{in}(\sigma, \theta) \;=\; \frac{S_{in}(\sigma, \theta, \boldsymbol{u}'_{10})}{\sigma} \tag{16}$$

The dissipation sink term can be split into bottom friction and whitecapping. Catastrophic wave breaking is not included in WAM since the model's assumptions no longer hold in the surf-zone. For the bottom friction sink, the presence of a current has no effect on the magnitudes of the wave-induced near-bottom velocities, (neglecting the complexities of a wave-current boundary layer), but the rate at which the alternating velocities are cycled through is affected by the modified ω. Bottom friction losses should be calculated using ω since the mechanism is caused by motion relative to the fixed bed. $S'_{bf}(\sigma, \theta)$ can therefore be estimated by calculating ω from $(\sigma \;+\; \boldsymbol{k} \cdot \boldsymbol{U})$, then setting

$$S'_{bf}(\sigma, \theta) \;=\; \frac{S_{bf}(\omega, \theta)}{\sigma} \tag{17}$$

The standard WAM parallelization of whitecapping dissipation does not include the relative wind velocity, so it remains reasonable to use this algorithm to estimate $S_{wc}(\sigma, \theta)$. A similar argument applies to the nonlinear interaction term. Since all wave components are shifted in frequency-space by the same current, each $S_{nl}(\sigma, \theta)$ can be estimated using the same algorithm as before.

The modifications of the WAM source/sink terms in this section have not yet been implemented. The changes should be coded and evaluated by the end of PET CWO project year 2 (3/31/98).

3.1.3 Implementation of unsteady currents in WAM

The WAM cycle 4 model includes the current effects on propagation detailed in Section 3.1.1, but unsteady currents are not permitted. An initial current field is read in and it is assumed that this field is representative for the duration of the simulation. A provision for unsteady currents has now been implemented by adding the input of currents every `N` propagation time steps, with `N` specified by the user. The current-related propagation and refraction terms are now re-calculated each time through the propagation loop.

Figure 7 (Gunther et al., 1992) shows the call tree of the main WAM cycle 4 module,CHIEF. A call to current input routine `WAMCUR`, taken from WAM pre-processing module `PREPROC`,

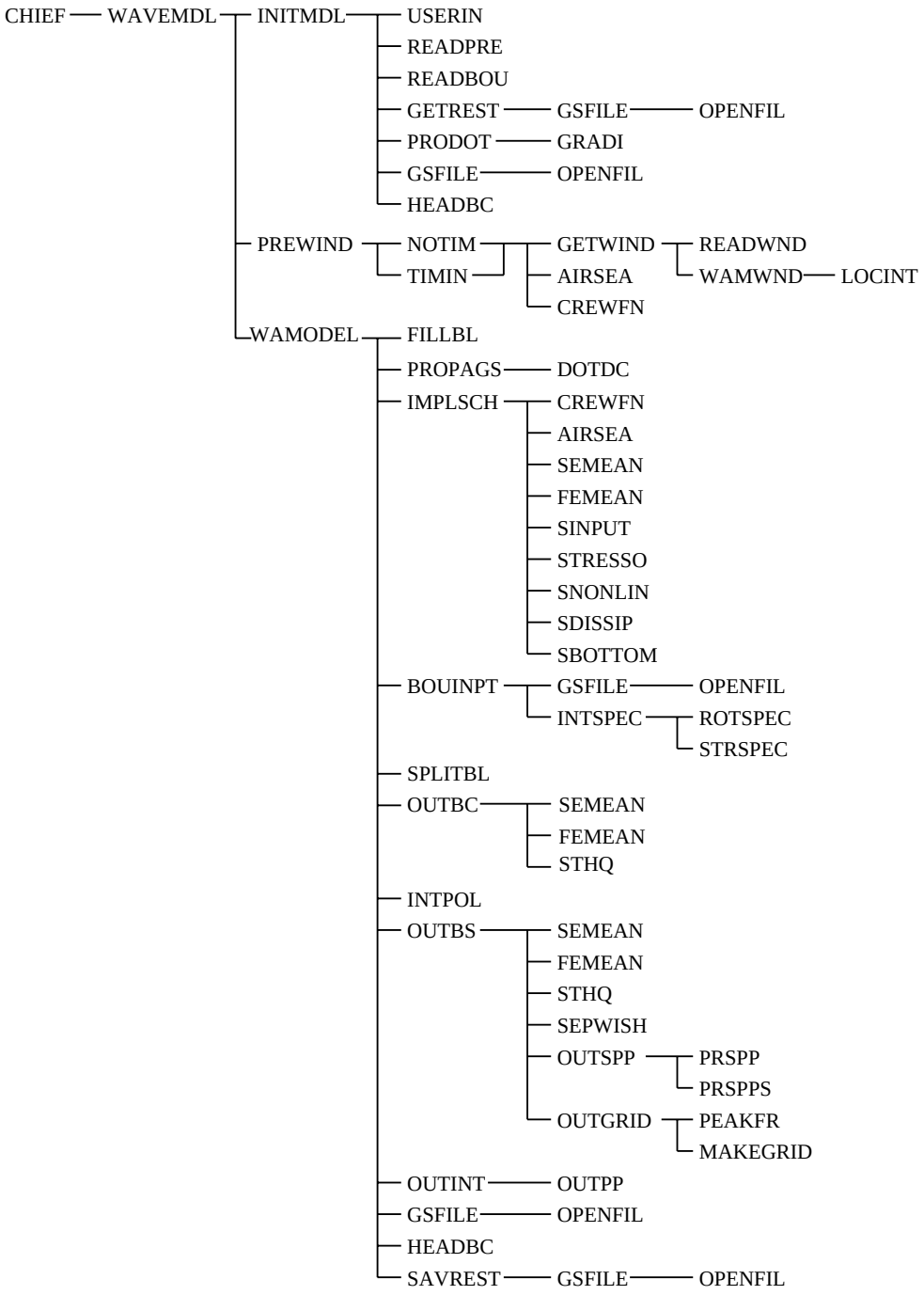

Figure 7: WAM model cycle 4 call tree (Gunther et al., 1992)

has now been added after the call to OUTINT; this updates the currents to be used at the next propagation time step. In the propagation loop, executed by WAMODEL, a slightly modified version of routine PROPDOT, named PROPDOT2, updates the current-effect arrays. PROPDOT is taken from the simulation initialization loop of CHIEF. The propagation routine, PROPAGS, has now been modified slightly to PROPAGS2; this version no longer uses routine DOTDC to read the current-effect arrays from buffer storage.

3.1.4 Implementation of unsteady depths in WAM

The WAM model has also been modified to accept unsteady depths. In the coupled CH3D/WAM system the unsteadiness is a result of the modulation of the water level due to circulation effects such as storm surge and drawdown. A field of water level fluctuations is now input to WAM every N propagation time steps, as with unsteady currents. This field is used to update the depth field, and depth-related refraction terms are now re-calculated each time through the propagation loop.

New routines READETA and DEPADD input the water level fluctuations and update the depths, respectively. READETA is similar to the current input routine READCUR called by WAMCUR, referred to in Section 3.1.3. The PROPDOT2 routine described in Section 3.1.3 updates the depth refraction arrays.

The test case described in Section 2.3.3 has been carried out for the 1-way coupled unsteady depths version of WAM (i.e. test I1S2, as defined in Section 2.3.3). CH3D water level fluctuations were read hourly from file, and current effects were switched off for clarity. Only very small differences resulted in the wave predictions. In shallow regions of highly tidal bodies of water, or nearshore regions subjected to hurricane and storm surge however, the implementation of unsteady depths will be of significant importance.

3.2 Effects of the wave field on the current computation

Two effects from the wave motion are minimally required in the computation of current circulation: one is the contribution of the radiation stress S_{ij} associated with the wave motion to the moment fluxes and the other is the change of the surface wind stress due to the presence of the wave stress τ_{wave}. The radiation stress components are given by (Phillips, 1977)

$$S_{ij} \;=\; \rho_w g \int_0^{2\pi} \int_0^{\infty} \left[\frac{c_g}{c_p} \frac{k_i k_j}{k^2} \;+\; (\frac{c_g}{c_p} - \frac{1}{2}) \delta_{ij} \right] E(f,\theta)\; df\; d\theta \tag{18}$$

where c_g and c_p are the wave group and phase speed; f and θ represent frequency and direction; k is the scalar wavenumber; δ_{ij} is the Dirac delta function; and $E(f,\theta)$ is the wave energy density spectrum.

The wave-induced stress (and the related stress ratio x) are updated using

$$\tau_{wave} \;=\; \sum_{\theta} \sum_{f} \frac{\rho_w}{\rho_{air}}\, \epsilon\, \beta\, \omega \left(\frac{u_* \cos\theta}{c_p} \right)^2 E(f,\theta)\; \Delta f\; \Delta\theta \tag{19}$$

where u_* is friction velocity; ϵ is a dimensionless constant; and β is an elaborate function of u_*, c_p, and z_0 (full details are given in Janssen (1991)).

The momentum flux. The x and y components caused by the radiation stress S_{ij} are defined as

$$M_x = -\frac{1}{H\rho_w}\Big[\frac{\partial S_{xx}}{\partial x} + \frac{\partial S_{xy}}{\partial y}\Big] \tag{20}$$

$$M_y = -\frac{1}{H\rho_w}\Big[\frac{\partial S_{xy}}{\partial x} + \frac{\partial S_{yy}}{\partial y}\Big] \tag{21}$$

where H and ρ_w are the total water depth and water density. The momentum flux M_x and M_y are added to the x and y components of the original momentum equation. The implementation procedure is as follows:

(i**)** convert the units of kg-m-s (WAM model) for the M_x and M_y to g-cm-s (CH3D model).

(ii**)** multiply the M_x and M_y by $f/U_{\rm ref}$ to non-dimensionlize them. Here f and $U_{\rm ref}$ are the Coriolis factor (9×10^{-5} s^{-1}) and reference horizontal velocity in cm/s.

(iii**)** transforming the M_x and M_y onto the ξ, η curvilinear coordinates:

$$M_\xi = x_\xi M_x + x_\eta M_y \tag{22}$$

$$M_\eta = y_\xi M_x + y_\eta M_y \tag{23}$$

where x_ξ, x_η, y_ξ and y_η are the Jacobian elements of coordinate transformation.

(iv**)** respectively adding M_ξ and M_η to the corresponding equations of the external mode in CH3D (Eqs. 31 and 32 in Chapman et al. (1996)), which are implemented in the subroutine `CH2DXY`.

Inclusion of wave-induced stress τ_{wave} to the total stress τ_{total} driving the current circulation: the total stress is defined as:

$$\tau_{total} = \tau_{wind} + \tau_{wave} \tag{24}$$

In case of no wave, the surface wind stress is the total stress and computed by:

$$\tau_{wind} = \rho_{air} C_{wind} |U_{10}| U_{10} \tag{25}$$

where ρ_{air} is the air density (1.225 kg/m^3), $C_{wind} = 10^{-3} \times (0.75 + 0.067 * |U_{10}|)$ and $|U_{10}|$ is the wind velocity at the height of $10m$ above the water surface.

When the effect of wave motion is considered, the wave-induced stress is computed using Eq. 19 for computing the total stress we have considered two approaches. One approach is similar to that of Li and Zhang (1997), but a fraction of the wave-induced stress is added to the total stress. The other is the same as that of (Janssen, 1991), which determines the total stress in an iterative way by updating the drag coefficient C_D as waves grow. This approach assumes that the effects of waves may be represented by an effective roughness length and goes in the following procedures.

Approach 1 is similar to that of Li and Zhang (1997), but a scale factor α $(0 < \alpha < 1)$ is multiplied to the wave-induced stress τ_{wave}, i.e.

$$\tau_{total} = \tau_{wind} + \alpha \times \tau_{wave} \tag{26}$$

The introduction of the α here is to realistically account for the wave effects by tuning a reasonable α. In Li and Zhang (1997) where $\alpha = 1$ was used, the wave effect may be overestimated.

Approach 2 computing the total stress follows the procedures:

(*i***)** For a given ratio of the wind-induced stress to the total stress ($x = \tau_{wave}/\tau_{total},\ x = 0$ is used in starting the integration in time), the wind drag coefficient is related to the ratio x by:

$$C_D = \left[\kappa/\ln\Big(\frac{L\sqrt{1-x}}{z_o}\Big)\right]^2,\ x\ <\ 1 \tag{27}$$

with $L = 10$ m, κ being the von Karman constant and z_o a typical roughness length of the wind profile.

(*ii***)** The total stress is updated using the standard formula:

$$\tau_{total} = \rho_{air} C_D |U_{10}| U_{10} \tag{28}$$

(*iii***)** The wave-induced stress is updated using Eq. 19.

(*iv***)** The procedure of *i* to *iii* is repeated until the integration time is ended.

In this approach, the total stress τ_{total} depends on the wind velocity, the wave-induced stress and the typical roughness length of the wind profile z_o. In the computation the value of z_o is tuned such that $C_D = C_{wind}$ for small x. For a uniformly distributed wind velocity of 10 cm/s, $z_o = 0.25$ mm is used, which yields a C_D of 0.00142 for small x and $C_D = 0.0045$ for $x = 0.9999$, which is the upper bound of wave to total-stress ratio.

The most important question to address scientifically is how to parameterize the wave-wind stress partitioning, the driving force in the wave-current coupling system. This needs more study, but it is out of the scope of this report.

The coding of including the wave-induced stress is implemented in the subroutine `CH3DWS`, where the wave-induced stress and also the momentum flux caused by the radiation stress are updated at the time frequency of once per `N` time steps. The effect of radiation stress or wave stress can be investigated individually. Once can also include both of them in the computation. An control parameter `IWAVE` is set for choosing an option of choosing the wave effects on the current computation.

3.3 One-way coupling of CH3D-s and WAM-s

After developing the physics formulae of the wave-current interaction and implementing them correspondingly in the WAM-s and CH3D-s codes, simple one-way coupling between the two models was investigated. The objective was to individually and quantitatively evaluate the coupling frequency and the impact of the wave field on the currents and vice versa.

The one-way coupling is realized through writing and reading files, in which the output is saved. As two step computations is involved.

- The WAM-s and the CH3D-s models are independently run for the same given wind field and the same horizontal grid mesh (Figures 1). During the run, WAM-s prints out the radiation stress and wave-induced stress once every `N` time steps and the CH3D-s prints out the horizontal velocity components and the water displacement at the surface at the same time frequency and the same time instant.

- The WAM-s and the CH3D-s are independently run with CH3D-s reading in the radiation stress and wave-induced stress at the same time as they were printed followed by a computation of the current circulation taking into account the wave's effects. In the same fashion WAM-s reads in the current velocity and water displacement at the surface and computes the wave propagation including the effects of the unsteady circulating currents.

The effects of including the wave field (or unsteady current circulation) on the current (or wave propagation) computation are evaluated by comparing the results of the runs with and without including the wave field (or unsteady current circulation). As reported in the previous studies (Li and Zhang, 1997; Mastenbroek et al., 1993), the effects are significant from both perspectives.

3.4 Two-way coupling of CH3D-s and WAM-s

By two-way coupling we mean that at every or every N time steps $N \geq 1$ not only the effect of the wave presence at the water surface is taking into account in the computation of the current circulation, but also the effect of the current circulation is in turn included in the computation of wave propagation. Compared to the one-way coupling, which isolates each of the two effects, the two-way coupling is fully dynamical and can more realistically represent the natural wave-current interactions.

From the programming stand point, there are a few ways to carry out the two-way coupling between CH3D-s and WAM-s. The ideal way would be to form a new code by reorganizing and putting the two codes together. Obviously, this would take a lot of laboring time. On the other hand, our study focus of the two-way coupling of the sequential codes is on the physics understanding of the wave-current interactions. Hence, we employed a very primitive, but the quickest way towards to objective to carry out the dynamical coupling as soon as possible. The two-way coupling is made through interactively writing the data to and reading the data from files. The codes have been modified such that at every N time steps $N \geq 1$, they can write out and read in the necessary data for the coupling.

3.4.1 Synchronization of the CH3D-s and WAM-s computations

The crucial technical point to achieve a real interactive two-way coupling lies on the synchronization of the CH3D-s and WAM-s computations at every or every N time steps. In the following we would briefly describe our synchronization procedure.

(i**)** We create 4 files, two for the writing and reading control (one for WAM-s and one for CH3D-s) and two for storing the necessary data, and run the WAM-s and CH3-s as simultaneously as possible.

(ii**)** At the first N time step, the CH3D-s writes the surface velocity and displacement (U,V and S) and writes a control variable informing WAM-s to start reading. In parallel, the WAM-s writes the radiation stress (RS) and wave stress (WS) and writes a control variable informing CH3D-s to start reading.

(iii**)** At the N+1 time step, the CH3D-s reads in the RS and WS and writes a control variable informing WAM to start writing again; the WAM-s reads in the U,V, and S and writes a control variable informing CH3D-s to start writing.

(iv**)** At the JxN time step (J=1,2,3, ...), both the CH3D-s and WAM-s write out the necessary data. In order to ensure the synchronized writing, the CH3D first checks whether the WAM has finished its previous time-step reading. If not, sleep for 0.1 second and checks again until the reading is finished. Then, CH3D-s writes out the newly computed U,V and S and writes a control variable informing WAM-s to start reading. The same process is made for the WAM-s' writing.

(v**)** At the JxN+1 time step, both the CH3D-s and WAM-s read in the data. The CH3D first checks whether the WAM has finished its previous time-step writing. If not, sleep for 0.1 second and checks again until the writing is finished. Then, CH3D-s reads in the newly computed RS and WS and writes a control variable informing WAM-s to start writing. The same reading process is made for the WAM-s too.

The procedure of iv and v is repeated until it reaches the end of the simulation time. So far the two-way coupling between CH3D-s and WAMS has been tested for the coupling time frequency of once per hour and for the test case of I1S1 described in section of 2.3.3. We plan to perform a series of runs to systematically examine the effects of the two-way dynamical coupling on the hydrodynamics of coastal computation, which will be reported by March 31, 1998.

3.5 Demonstration Examples

3.5.1 CH3D Results

One-way coupling between CH3Ds and WAMs has been tested for an idealized case of I1S1, which is described in the first paragraph of Section 2.3.3. We individually examined the effects of including the wave radiation stress and the wave-induced stress. It is found that the inclusion of the wave-induced stress can produce great effects on the current circulation while the effect of the wave radiation stress are not significant. We also examined the importance of wave-wind stress

partitioning in driving the current circulation. It turns out the two approaches taking into account the effect of wave-induced stress as described in Section 3.2 work in the same way to influence the current circulation, but with a different intensity depending on the value of the α used in Eq. 26.

Figure 8 shows the spatial distribution of the current velocity and water displacement at the surface and at different simulation time in case of no wave motion considered. The maximal and minimal values of U and V at that time instant are marked in each panel. These results set the reference to demonstrate how and how much the presence of wave motion will affect the current circulation.

Figure 9 shows the same physical fields as Figure 8, but with the wave-induced stress included and updated once each hour. In this run, the total stress is computed using **Approach 1** for $\alpha = 1.0$. The effects of including the wave-induced stress on the velocity and water elevation are illustrated in Figure 10, which are obtained by subtracting the results with no-wave (shown in Figure 8) from the corresponding ones with wave field (shown in Figure 9). One can observe that the changes caused by the wave-stress have the same magnitude as those shown in no-wave case (Figure 8). We also ran a test using **approach 1** to computed the total stress, but with $\alpha = 0.5$. As expected, the changes due to the wave presence become smaller for a smaller α.

Figure 11 shows the same physical fields as Figure 8, but with the total stress computed using **Approach 2**. Compared to Figure 9, one can find the physical fields are quite similar, but the intensities are larger in Figure 9. Figure 12 shows the effects of using Approach 2; the fields were obtained by subtracting the results in Figure 8 from those in Figure 11.

3.5.2 WAM Results

Results are presented in this section for WAM-s case I1S2. This is the same test as I1S1 in Section 2.3.3, but with one-way coupling added in the WAM-s propagation scheme using CH3D-s currents read from file. The currents were input once an hour, meaning N in Section 3.1.3 was set to 60.

Figure 13 shows a contour plot of H_s at hour-36 of test I1S2. Comparing this plot with Figure 4, one can see that the addition of the currents has increased the wave height slightly. Holthuijsen and Tolman (1991) used currents from an idealized Gulf Stream ring in a wave model similar to WAM-s. It was concluded there that currents aligned with waves should reduce H_s and increase mean wave frequency, $\overline{f}$. The currents in test I1S2 tended to be on the order of 0.15 m/s and aligned 30 to 45 degrees to the right of the outgoing wind direction, (the rotation is a combination of Coriolis and bathymetry effects). The H_s effect in Holthuijsen and Tolman (1991) has, therefore, been reversed here, though the frequency modulation is in agreement. Figures 14 shows time series of H_s at station 8 (grid point 23,16) for tests I1S1 and I1S2. The slight increase in H_s for the partially aligned currents is again seen.

A second idealized test was used to confirm the effect of current-related propagation on H_s. In this test, "I2", a 5 m/s N wind was applied to the Lake Michigan grid for 24 hours. To clarify the current effects, idealized currents were also now used, rather than CH3D-s currents. Two versions of the nominally one-way coupled test were run; in "I2N" a steady 0.5 m/s current from the North was applied, while in "I2S" a 0.5 m/s Southerly current was used.

Figure 15 shows time series of H_s at station 8 for tests I2N and I2S.

The plot confirms that steady currents aligned with waves in WAM-s lead to increased wave

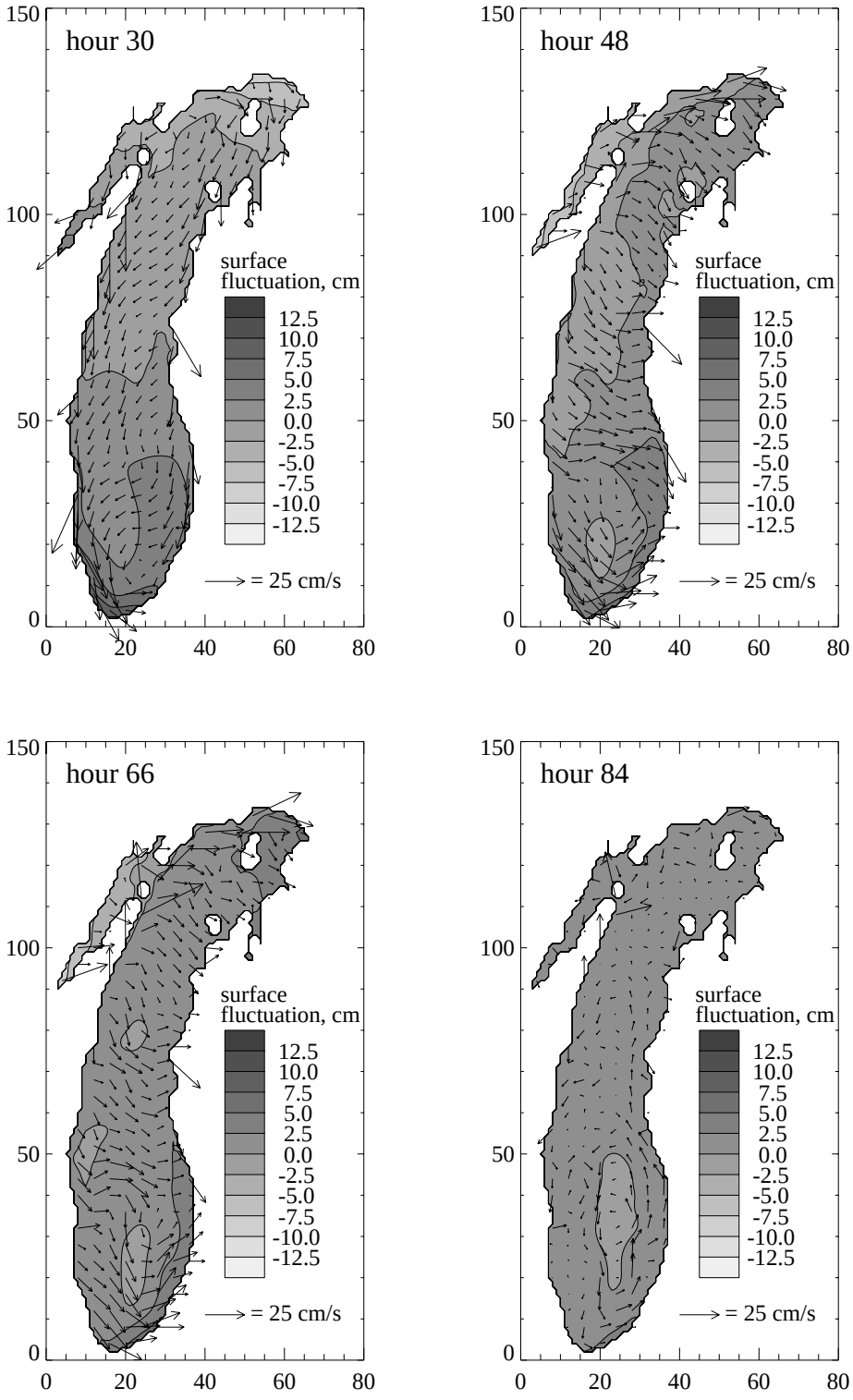

Figure 8: Temporal variations of the surface velocity (indicated by arrows) and water surface elevation (greyscale map) for test case of I1 at the simulation time of 30 hour (panel upper-left), 48 hour (upper-right), 66 hour (lower-left) and 84 hour (lower-right). In this run no wave motion is included.

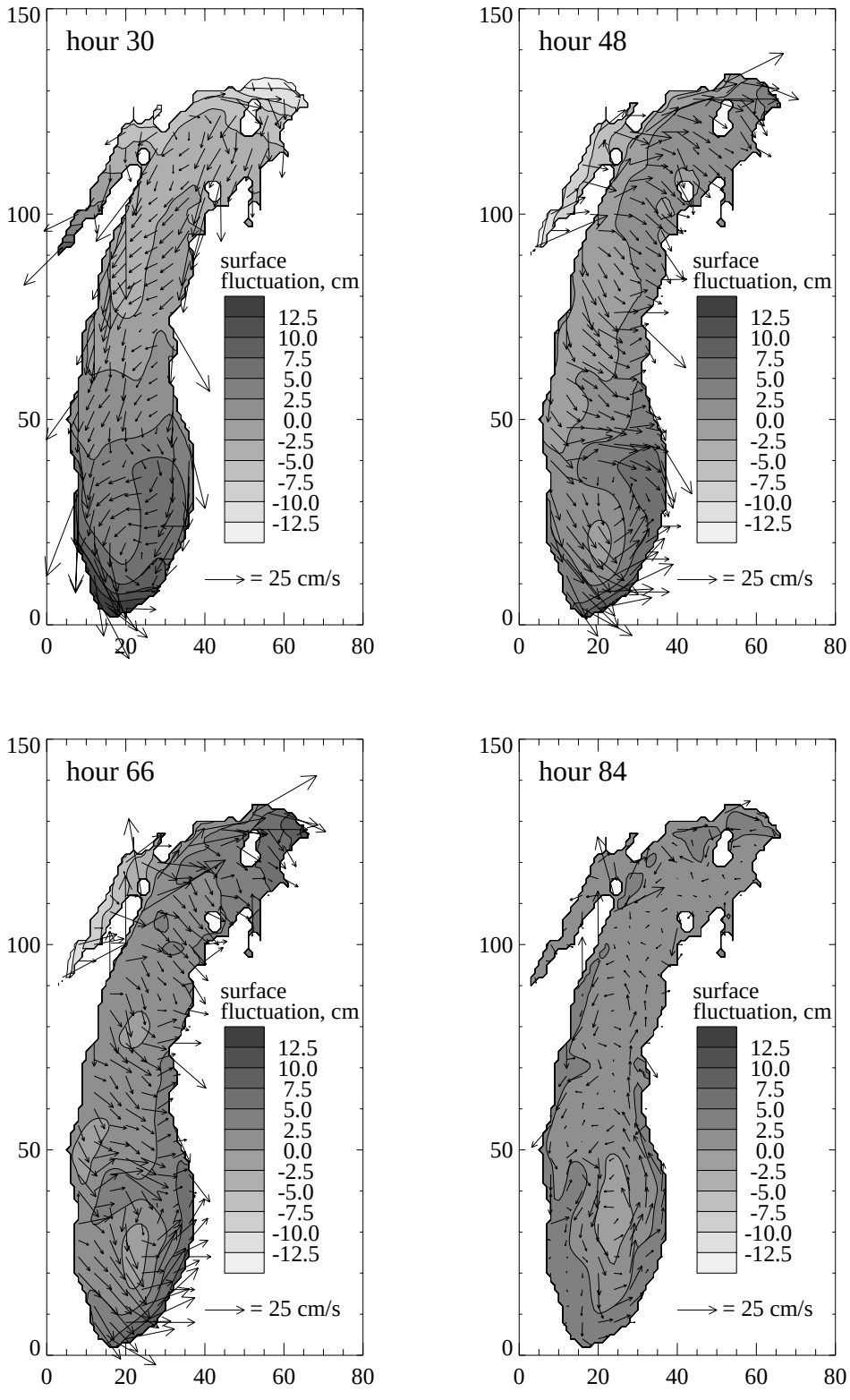

Figure 9: Same as Figures 8, but the wave-induced stress computed using Approach 1 for $\alpha = 1$ is coupled and updated once each hour.

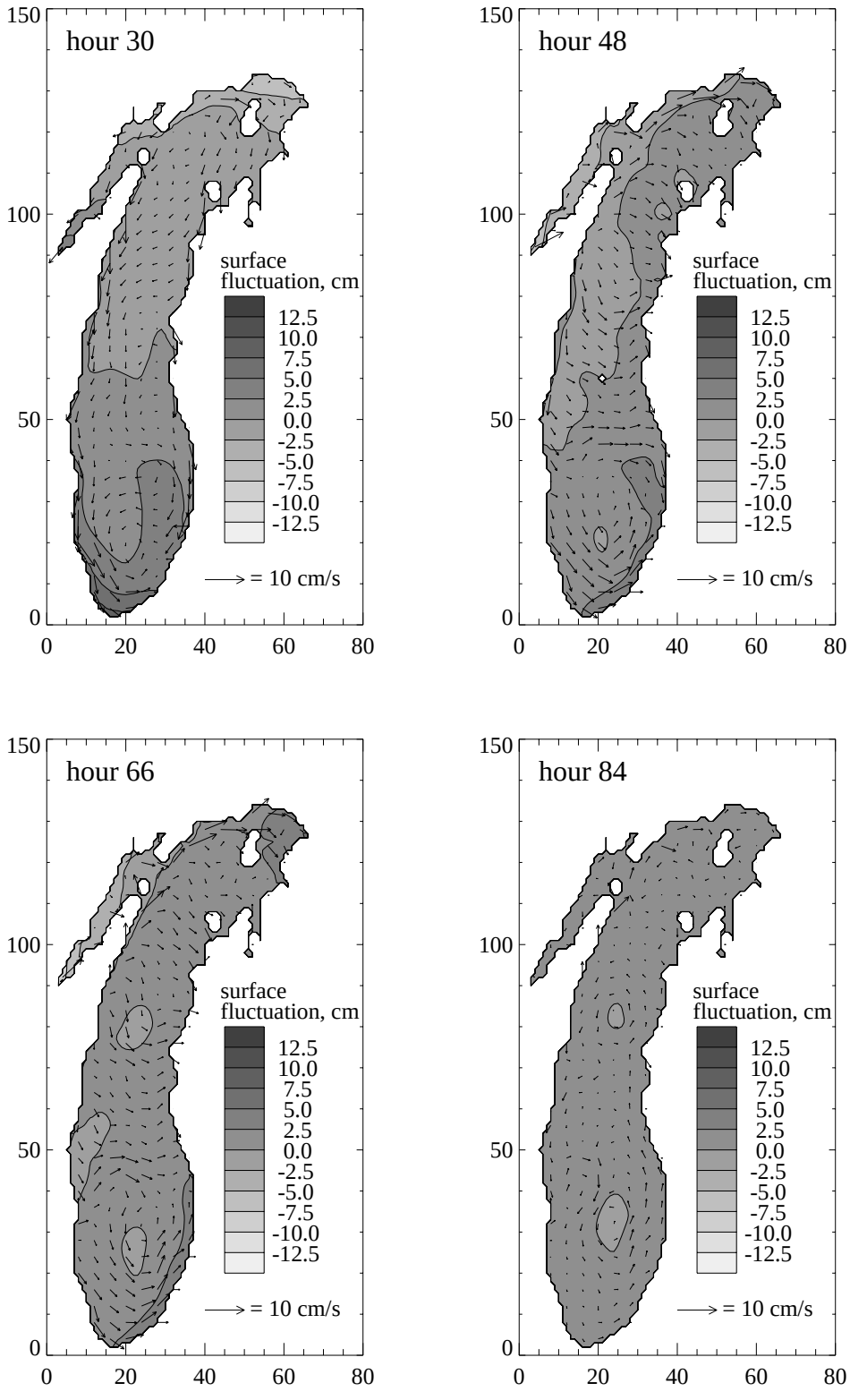

Figure 10: Effects of including wave-induced stress for Approach 1 with $\alpha = 1$ on the surface velocity (the arrows) and water surface elevation (greyscale map).

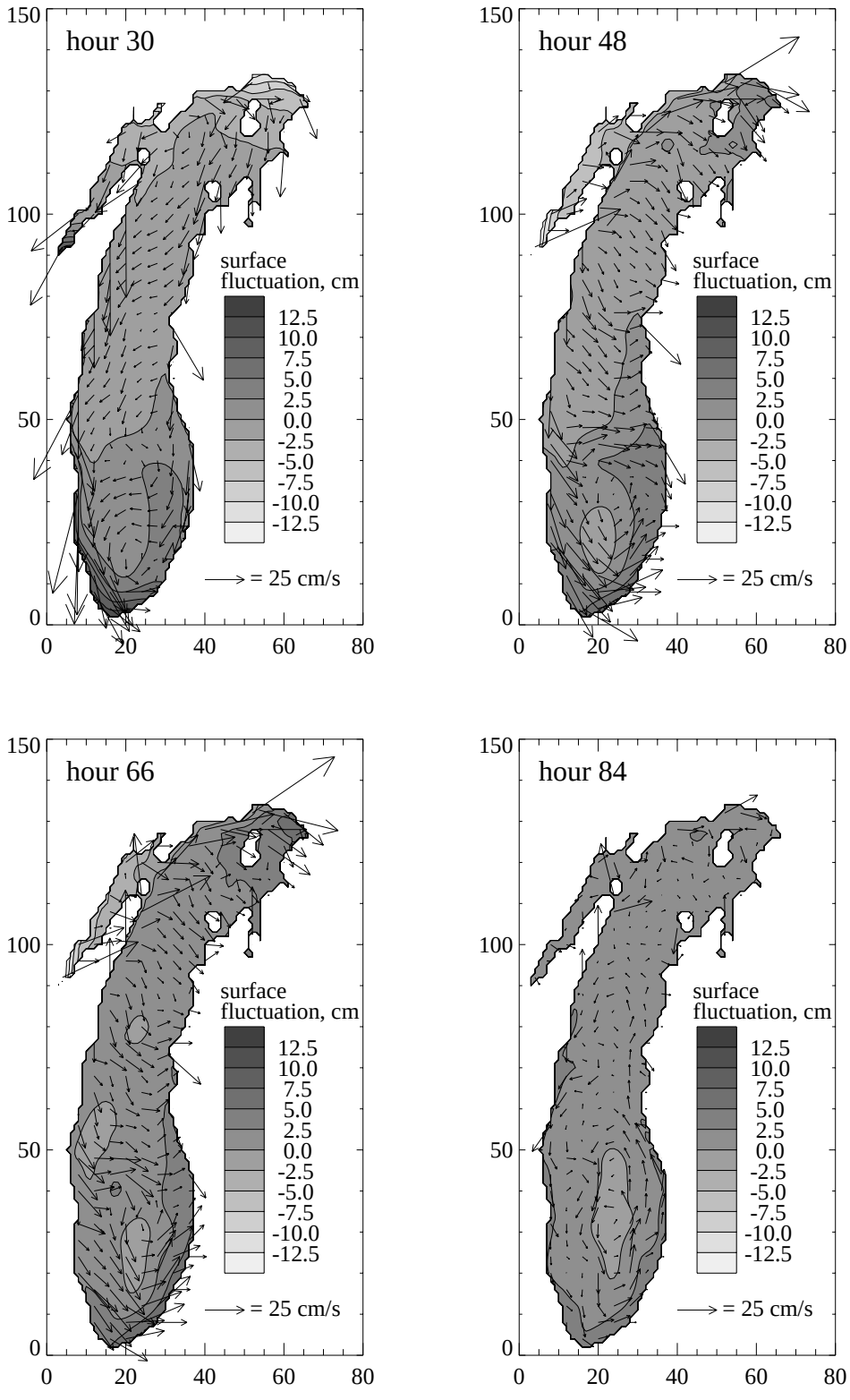

Figure 11: Same as Figures 8, but the wave stress computed using Approach 2 is coupled and updated once each hour.

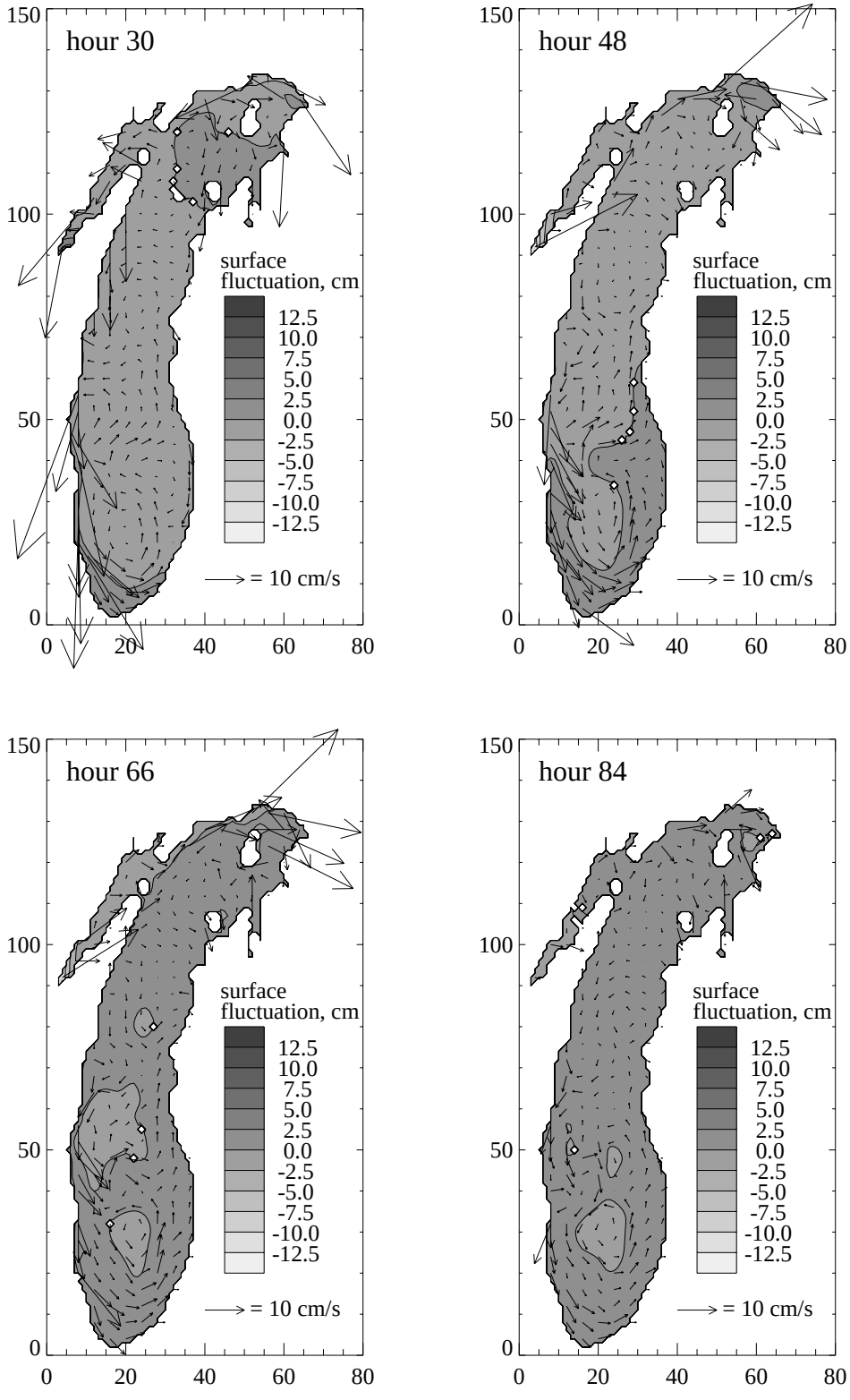

Figure 12: Effects of including wave-induced stress computed using Approach 2 on the current velocity (the arrows) and water surface elevation (greyscale map).

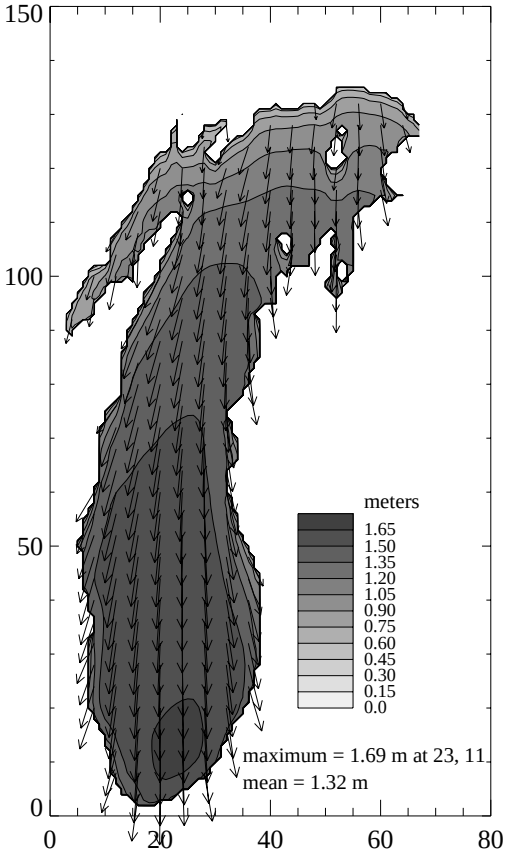

Figure 13: Significant wave height contours at hour-36 of test I1S2

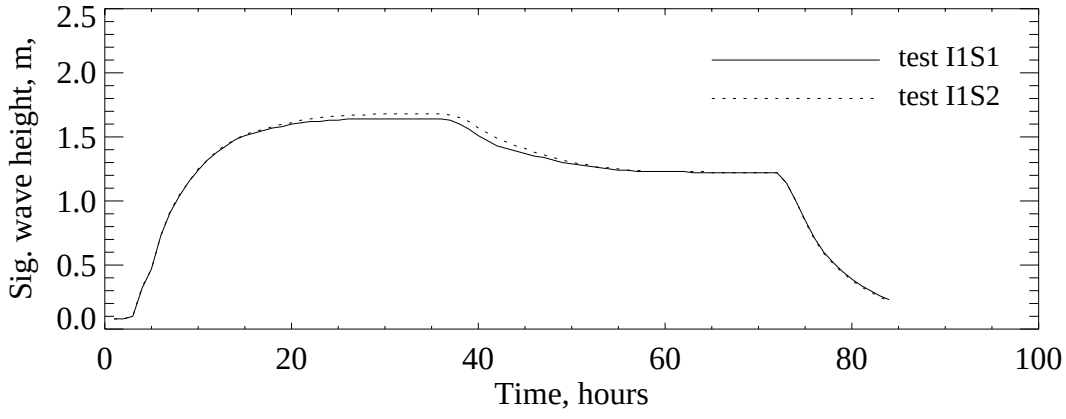

Figure 14: Significant wave height time series at station 8 for tests I1S1 and I1S2

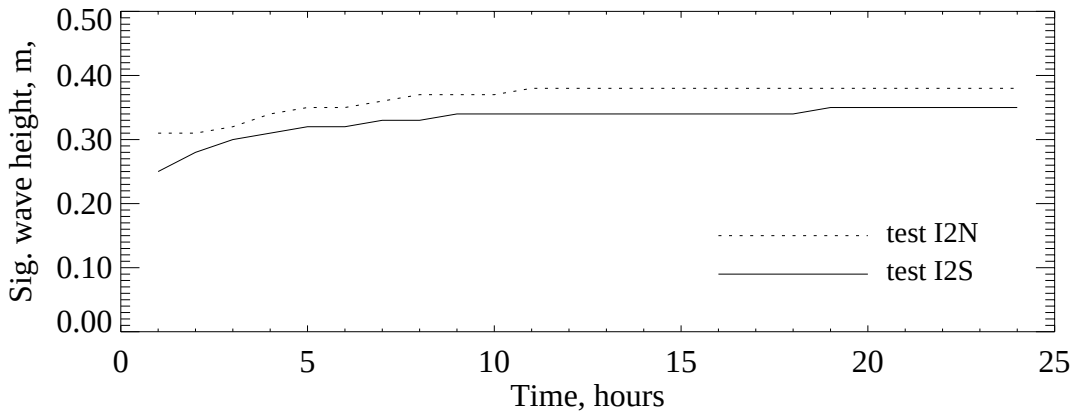

Figure 15: Significant wave height time series at station 8 for tests I2N and I2S

heights. The implementation of unsteady currents described in Section 3.1.1 is therefore not the cause of the unexpected H_s modulation. One expects waves to be smaller with an aligned current because the relative wind speed is reduced. This suggests that the reason H_s has increased in I1S2 (and I2N) is that the current effects on source/sink terms, described in Section 3.1.2, have not yet been implemented. The tests appear to confirm that the source/sink terms in WAM cycle 4 are not entirely consistent with the presence of currents in the model.

4 Plan for Year 3

- Continue to study the physics of the wave-current interactions.
- Examine the dynamical interactions among the wave, current and sediment transport.
- Couple WAM-p/CH3D-p test and apply to Lake Michigan.
- Parallelize the SED module.
- WAM/CH3D/SED Coupling in parallel form.
- Implement a mesoscale atmospheric modeling system (MM5) at CEWES.

Acknowledgement

This work was supported in part by a grant of HPC time from the DoD HPC Modernization Program

References

ASCE Task Committee on Turbulence Models in Hydraulic Computation (1988). Turbulence modeling of surface water flow and transport, *J. Hydraul. Eng.*, ASCE **114**(9): 1–1073.

Bedford, K. W. and Schwab, D. J. (1994). The Great Lakes Forecasting System: An Overview, *in* G. V. Cotroneo and R. R. Rumer (eds), *Hydraulic Engineering '94, Proceedings of the Conference*, ASCE, Buffalo, NY, pp. 197–201. See URL http://superior.eng.ohio-state.edu/.

Bedford, K. W. and Schwab, D. J. (1998). Recent Developments in the Great Lakes Forecasting System (GLFS) - Performance Evaluation, *Proceedings of the 78th Annual Meeting*, American Meteorological Society. in press.

Beletsky, D., O'Connor, W. P., Schwab, D. J. and Dietrich, D. E. (1997). Numerical simulation of internal Kelvin waves and coastal upwelling fronts, *J. Phys. Oceanogr.* **27**(7): 1197–1215.

Blumberg, A. F. and Mellor, G. L. (1987). A description of a three-dimensional coastal ocean circulation model, *in* N. S. Heaps (ed.), *Three-dimensional Coastal Ocean Models*, Coastal and Estuarine Sciences 4, American Geophysical Union, pp. 1–16.

Chapman, R. S., Johnson, B. H. and Vemulakonda, S. R. (1996). User's Guide for the Sigma Stretched Version of CH3D-WES; A Three-Dimensional Numerical Hydrodynamic, and Temperature Model, *Technical Report HL-96-21*, U.S.Army Engineer Waterways Experiment Station, Vicksburg, MS.

Glenn, S. M. and Grant, W. D. (1987). A suspended sediment stratification correction for combined wave and current flow, *J. Geophys. Res.* **92**: 8244 – 8264.

Gunther, H., Hasselmann, S. and Janssen, P. A. E. M. (1992). The WAM model cycle 4, *Technical report*, Deutsches KlimaRechenZentrum, Hamburg, Germany. WAM Report no. 4.

Haney, R. L. (1991). On the pressure gradient force over steep topography in sigma coordinate models, *J. Phys. Oceanogr.* **21**: 610–619.

Holthuijsen, L. H. and Tolman, H. L. (1991). Effects of the gulf stream on ocean waves, *Journal of Geophysical Research* **96**: 12755–12771.

Janssen, P. A. E. M. (1991). Quasi-linear theory of wind-wave generation applied to wave forecasting, *J. Phys. Oceanogr.* **21**: 1631–1642.

Johnson, B. H., Kim, K. W., Heath, R. E., Hsieh, B. B. and Butler, H. L. (1991). Development and verification of a three dimensional numerical hydrodynamic, salinity and temperature model of Chesapeake Bay, *Technical Report HL-91-7*, U.S.Army Engineer Waterways Experiment Station, Vicksburg, MS.

Komen, G. J., Cavalieri, L., Donelan, M., Hasselmann, K., Hasselmann, S. and Janssen, P. A. E. M. (1994). *Dynamics and Modelling of Ocean Waves*, Cambridge University Press, Cambridge, U.K.

Li, Y. S. and Zhang, M. Y. (1997). Dynamic coupling of wave and surge models by eulerian-lagrangian method, *J. Port, Coast., Waterway Harbors Eng.* **123**(1): 1–7.

Mastenbroek, C., Burgers, G. and Janssen, P. A. E. M. (1993). The dynamical coupling of a wave model and a storm surge model through the atmospheric boundary layer, *J. Phys. Oceanogr.* **23**: 1856–186.

Mortimer, C. H. (1963). Frontiers in physical limnology with particular reference to long waves in rotating basins, *Proceedings of the Sixth Conf. on Great Lakes Research*, Vol. 10, Great Lakes Research Division, University of Michigan, pp. 9–42.

Phillips, O. M. (1977). The sea surface, *Modelling and Prediction of the Upper Layers of the Ocean*, Pergamon Press, Elmsford, NY, pp. 229–237.

Spasojevic, M. and M. Holly, J. (1994). Three dimsnsional numerical simulation of mobile-bed hydrodynamics, *Technical Report HL-94-2*, U. S. Army Engineer Waterways Experiment Station, Vicksburg, MS.

Tolman, H. L. (1991). A third-generation wave model for wind waves on slowly varying, unsteady, and inhomogeneous depths and currents, *Journal of Physical Oceanography* **21**: 782–797.

WAMDI (1988). The WAM model - a third generation ocean wave prediction model, *Journal of Physical Oceanography* **18**: 1775–1810.

Welsh, D. J. S., Zhang, S., Sadayappan, P. and Bedford, K. W. (1998). Climate, weather and oceanography core support, year 2: WAM performance improvement and NLOM optimization, *Technical report*, The Ohio State University, Columbus, OH. Prepared for the Department of Defense HPC Modernization Program.